Producing a Digital Elevation Model Using a Cluster of Small-Aperture SAR Satellites: An Airborne Demonstration

Maxwell Nogueira Peixoto[a], Gerhard Krieger[a], Alberto Moreira[a], Christian Waldschmidt[b], Michelangelo Villano[a]
[a] German Aerospace Center (DLR), Microwaves and Radar Institute, Oberpfaffenhofen, Germany
[b] Ulm University, Ulm, Germany

Abstract

The generation of time series of digital elevation models (DEMs) is fundamental for monitoring and understanding fast dynamic processes on the Earth's surface. This work presents a novel concept for single-pass DEM generation based on a cluster of small-aperture synthetic aperture radar (SAR) satellites with different along- and cross-track baselines operating with a sub-Nyquist pulse repetition frequency. A key feature of the concept is the height retrieval algorithm based on a generalized maximum likelihood estimation, whose theoretical formulation is presented. A demonstration is then conducted using multi-baseline airborne data from DLR's F-SAR system. The first results show that the proposed concept is a promising solution for the generation of highly accurate DEMs robust to phase unwrapping errors in a single pass.

1 Introduction

Synthetic aperture radar (SAR) interferometry is a valuable remote sensing tool capable of supplying products with high accuracy and resolution for a wide range of applications in Earth observation [1]. Investigating and monitoring dynamic phenomena on the Earth's surface demands continuous time series with small revisit times [2], [3]. While nowadays frequent revisit SAR imaging is achieved by satellite constellations, time series of high-quality digital elevation models (DEM) at short time intervals are not yet available. Even state-of-the-art interferometric systems often require multiple passes of the satellites to generate unambiguous DEMs, severely limiting the frequency at which these products can be delivered. While TanDEM-X can acquire high quality interferograms in a single pass, producing an unambiguous DEM requires additional passes with different baselines, the separation between the satellites, to resolve unwrapping errors and layover, for example in mountainous areas [4], [5]. Multi-pass acquisitions also bring additional complexity to the product generation, as the observed scene evolves between the different passes. For example, topographic changes, such as a snow fall event, can prevent interferograms from different passes to be jointly used for resolving unwrapping errors.

In single-baseline across-track interferometry, the larger the baseline, the higher the DEM accuracy, but the more susceptible it is to phase unwrapping errors. The requirement of robustness to phase unwrapping errors then imposes an upper limit on the maximum baseline and so on the accuracy of the resulting DEM. TanDEM-X, for example, operates with baselines between around 250 m and 400 m, less than 10% of the critical baseline, due to this limit. Phase unwrapping errors can be resolved if multiple interferograms with different baselines are available, thus removing this upper limit on the baselines. Multi-baseline interferometry is then capable of generating DEMs robust to unwrapping errors and, through the use of larger baselines, with even higher accuracy. However, a system capable of single-pass multi-baseline interferometry would require at least three satellites flying in formation.

We propose a novel distributed concept for DEM generation in a single pass based on a cluster of small-aperture SAR satellites, which we have also recently patented [6], [7]. The system operates with a pulse repetition frequency (PRF) much smaller than the Doppler bandwidth, which allows the use of small-aperture antennas without compromising the swath width. A key feature of this concept is the processing technique for DEM generation. The proposed technique combines the data from all satellites to jointly resolve azimuth and height ambiguities without the need to generate unambiguous focused SAR images as an intermediate step. This removes the constraint of arranging the cluster in trains of satellites, enabling further cross-track baseline diversity, and using fewer satellites.

This work further presents a demonstration based on a dedicated multi-baseline airborne acquisition recently performed with the F-SAR system of the German Aerospace Center (DLR) over the Soiernspitze, near Mittenwald, Germany.

2 Concept and Processing

The proposed concept consists of exploiting a cluster of small-aperture SAR satellites for single-pass DEM generation with high accuracy and robustness to unwrapping errors. The pulse transmission can be alternated between some or all satellites of the cluster [8], or be handled by a dedicated satellite, allowing the others to be receive-only [9]–[11]. Multiple satellites can also transmit simultaneously [12]. The system observes a wide Doppler bandwidth due to the small antenna apertures, and operates with a PRF much lower than this bandwidth. Therefore, the data from a single receiver in the cluster cannot be used to form an unambiguous SAR image. The satellites in the cluster must be arranged with a combination of along-track and cross-

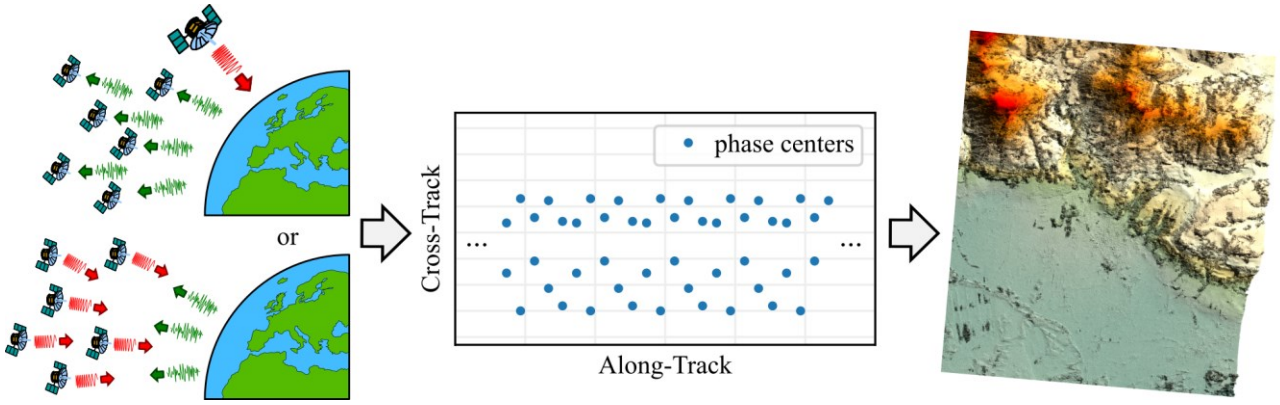

Figure 1 Cluster of small-aperture satellites used for distributed SAR interferometry, either with a dedicated transmitter (top left) or with multiple transmitters (bottom left). The data from all satellites in the cluster combined form an array of phase centers with a combination of along-track and cross-track baselines (center) that is processed to directly generate a DEM (right) without the intermediate step of forming unambiguous SAR images.

track baselines. The former enables the suppression of azimuth ambiguities similarly to distributed SAR imaging, where the data from a train of SAR satellites operating with a sub-Nyquist PRF is combined to form an unambiguous SAR image [8]–[11], [13], [14]. The latter allows for the generation of a DEM robust to unwrapping errors in a single pass as in conventional multi-baseline interferometry. The larger cross-track baselines provide accuracy to the DEM while the smaller and intermediate baselines provide robustness to unwrapping errors. While a formation with three trains of satellites with distributed SAR imaging would achieve the goal of single-pass DEM generation with high accuracy, typical terrain has a much lower information content than three unambiguous SAR images, indicating that the same goal can be achieved with less data. This observation was first exploited in [15], [16], where one or more SAR CubeSats are added in formation with a bistatic interferometer and are used to resolve unwrapping errors despite the high noise and ambiguity levels of the CubeSat images. Here we exploit this by employing clusters not arranged in trains of satellites, achieving increased cross-track baseline diversity and using fewer satellites, as small and intermediate cross-track baselines can be less populated. This is supported by a novel processing scheme that, as depicted in **Figure 1**, combines the data from all satellites in the cluster to produce the DEM without the need to form unambiguous SAR images as an intermediate product.

As shown in **Figure 2**, as a first step a highly ambiguous SAR image is produced for each transmitter/receiver pair. The azimuth compression includes the reconstruction of the wide Doppler bandwidth larger than the PRF. It can also include additional processing for the suppression of azimuth ambiguities, such as adaptive spectral filtering exploiting estimates of the local azimuth-ambiguity-to-signal ratio, which can be obtained by adapting the technique in [17]. The reconstructed Doppler bandwidth is a multiple of the PRF and is split into sub-bands with width equal to the PRF. Then multilooked interferograms between all possible pairs of SAR images and for each sub-band are formed. These interferograms then compose the estimated covariance matrices of the stack of highly ambiguous images:

$$\hat{C}_b(R,y) = \frac{1}{N_L}\sum_{l=1}^{N_L} \boldsymbol{u}_{b,l}(R,y)\boldsymbol{u}_{b,l}^H(R,y) \tag{1}$$

where b is an index indicating the sub-band — the sub-band b is offset by $b \cdot \mathrm{PRF}$ from the central band —, R is the slant range, y is the azimuth, N_L is the number of looks, and $\boldsymbol{u}_{b,l}(R,y)$ is a vector of pixels, one from each highly ambiguous image at the band b and the look l. Finally, the DEM is jointly estimated from all covariance matrices. Specifically, for each pixel in range and azimuth, the height is obtained through a generalized maximum likelihood estimation that considers as parameters the heights, noise-free coherences, and backscatters of the main and azimuth-ambiguous components of the covariance matrices. A model for the covariance matrix C_b is derived as the sum of the contributions of the main $C_{b,0}$ signals, the ambiguous signals $C_{b,\rho}$, and the noise C_{noise}:

$$C_b(\boldsymbol{\theta}) = C_{b,0}(\boldsymbol{\theta}_0) + \sum_{\rho\neq 0} C_{b,\rho}(\boldsymbol{\theta}_\rho) + C_{\mathrm{noise}} \tag{2}$$

where ρ is the ambiguity order, with $\rho = 0$ indicating the main signal, $\boldsymbol{\theta}_\rho$ is a vector containing the height h_ρ, the noise-free coherence γ_ρ, and the beta naught β_ρ^0 for the respective ambiguity order, and $\boldsymbol{\theta}$ is a vector containing these parameters for all ambiguity orders. To reduce the number of parameters of the estimation, the noise-free coherence is assumed to be independent of the across-track baseline. The elements $c_{b,\rho,nm}$ of the covariance matrix $C_{b,\rho}$ are modeled as

$$\begin{aligned} c_{b,\rho,nm}(\boldsymbol{\theta}_\rho) &= A_{b,\rho}\beta_\rho^0\gamma_\rho e^{j2\pi(b-\rho)\frac{y_{s,nm}\mathrm{PRF}}{v_s}} e^{jk_{z,nm}h_\rho}, \quad \text{if } n \neq m, \\ c_{b,\rho,nm}(\boldsymbol{\theta}_\rho) &= A_{b,\rho}\beta_\rho^0, \qquad \text{if } n = m, \end{aligned} \tag{3}$$

where $y_{s,nm}$ and $k_{z,nm}$ are, respectively, the along-track baseline and the vertical wavenumber between the pair of images of indices n and m, v_s is the platform speed, and $A_{b,\rho}$ is the factor by which the antenna pattern affects the

intensity of the respective ambiguity at the respective sub-band. The infinite sum in (2) can be truncated at the ambiguity orders where the $A_{b,\rho}$ terms become negligible. The log-likelihood function is then

$$\ln L(\boldsymbol{\theta}) = \sum_b -\operatorname{tr}\left(C_b^{-1}(\boldsymbol{\theta})\hat{C}_b^H\right) - N_L \ln|C_b(\boldsymbol{\theta})| - N_L N_s \ln \pi, \quad (4)$$

where $|\cdot|$ denotes the matrix determinant, and N_s is the number of images in each sub-band. Finally, the height is estimated by finding the parameters $\widehat{\boldsymbol{\theta}}$ that maximize this log-likelihood function,

$$\widehat{\boldsymbol{\theta}} = \underset{\boldsymbol{\theta}}{\operatorname{argmax}} \ln L(\boldsymbol{\theta}), \quad (5)$$

and discarding all the parameters other than the height of the main signals, $\widehat{h_0}$. This method for producing DEMs is a generalization of conventional SAR interferometry. In fact, it is exactly equivalent to it in the single-baseline case when unambiguous images are available. In the multi-baseline case where unambiguous images are available, this method is equivalent to the maximum-likelihood height estimation [18].

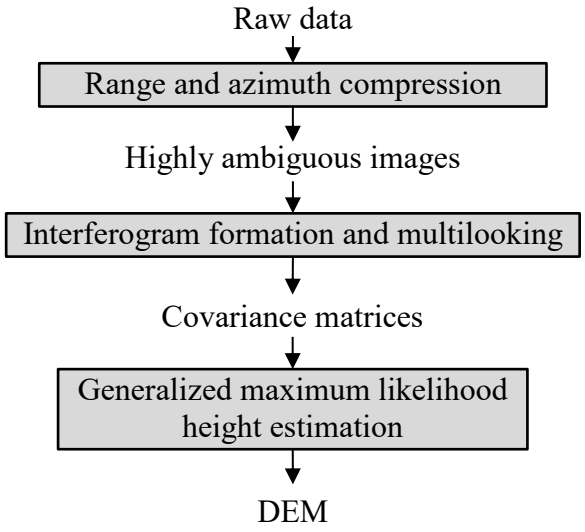

Figure 2 Block diagram of the processing scheme for DEM generation using a cluster of small-aperture SAR satellites operating with a PRF much lower than the Doppler bandwidth.

3 F-SAR Experiment

A dedicated airborne SAR campaign over the Soiernspitze, near Mittenwald, Germany, was performed using DLR's F-SAR system to demonstrate the novel distributed concept for single-pass generation of highly-accurate DEMs. One of the acquired F-SAR images is shown in **Figure 3**. The test site contains diverse topography with mountainous and flat areas, both with and without vegetation cover, allowing the evaluation of the performance in diverse scenarios. The data were acquired in the L, S, and X bands in 10 parallel tracks arranged as shown in **Figure 4** at an altitude of 6,705 m above the WGS84 ellipsoid. The position of the tracks was chosen to provide multiple heights of ambiguity in the range of 10 to 200 m in both L and S bands. Furthermore, a PRF much higher than the Doppler bandwidth was employed, so that data are oversampled in azimuth. This work considers the L-band data.

The data that would be acquired by a distributed SAR interferometric system with 8 receivers dispersed with along- and across-track baselines as indicated in **Figure 5** were simulated from the F-SAR images. The Doppler bandwidth of the system is 189 Hz and the PRF is equal to one third of this bandwidth, i.e., 63 Hz. The data from each receiver were simulated by first filtering the F-SAR image of the receiver's track to the bandwidth of 189 Hz and removing

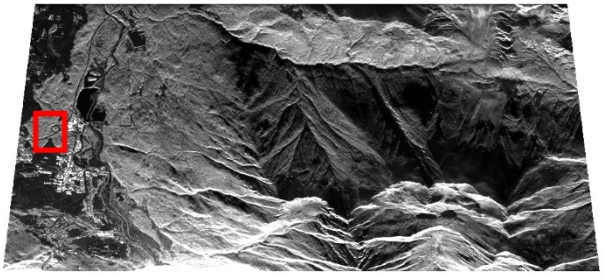

Figure 3 L-band image formed from track number 1. The red rectangle delimits the region on which the DEMs presented in this section were generated.

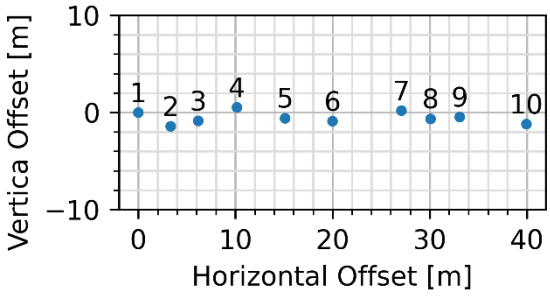

Figure 4 Vertical and horizontal offsets (blue points) in the cross-track plane of the 10 parallel tracks of the F-SAR acquisition with respect to the track number 1, which is at an altitude of 6,705 m. The identifier of each track is shown above the respective track.

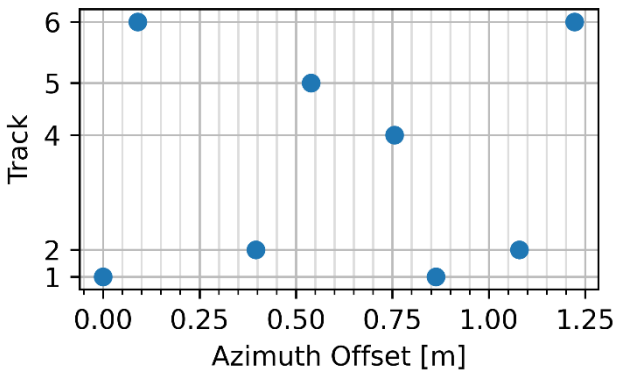

Figure 5 Spatial arrangement of the 8 receivers (blue points) of the simulated distributed SAR interferometric system.

the Doppler centroid resulting from the squinted geometry, then translating it in azimuth according to the azimuth offset of the receiver, then performing inverse focusing along azimuth to simulate the range-compressed data, and finally downsampling the range-compressed data by a factor of three to achieve the desired PRF.

The data from all the receivers of the distributed SAR interferometric system were then focused to produce highly ambiguous images and recover the wider Doppler bandwidth equal to three times the system's PRF. Three Doppler sub-bands, [-3PRF/2, -PRF/2[, [-PRF/2, PRF/2[, and [PRF/2, 3PRF/2[, all with width equal to the system's PRF, were reconstructed and processed independently. A TanDEM-X DEM was used for compensating the flat earth and topographic phases, so that all derived height measurements are height offsets with respect to the TanDEM-X DEM. The interferograms formed between the highly ambiguous images were multilooked by averaging across range and azimuth, with 9 × 3 pixels, respectively. Finally, the generalized maximum likelihood estimation was performed as indicated in (5), but with a further simplifying assumption that all noise-free interferometric coherences γ_ρ are 0.9. The estimated height of the main component was used to form a DEM, whereas the other parameters were discarded.

The results are presented for the region outlined by the red rectangle in **Figure 3**. This region of the SAR image is shown in **Figure 6**. The DEM obtained with the proposed distributed interferometric system is shown in **Figure 7** (a). It shows good agreement with the reference DEM shown in **Figure 7** (b), formed through multi-baseline interferometry considering the fully-sampled images of the same tracks used for the proposed system (see **Figure 5**). The proposed technique also present outlier pixels with very incorrect height estimates. These outliers are caused by the presence of azimuth ambiguities and by failure of the global optimizer used to solve the generalized maximum likelihood problem. Note, comparing **Figure 7** (a) and **Figure 6**, that the outliers are concentrated in low-backscatter areas. These outliers can be detected and potentially eliminated by reprocessing with a more robust global optimizer. The statistics of the height difference between the two DEMs in **Figure 7** was evaluated in the region outlined by the black rectangle and ignoring the outlier pixels. The standard deviation of the height difference was found to be 1.5 m, while the bias was negligible.

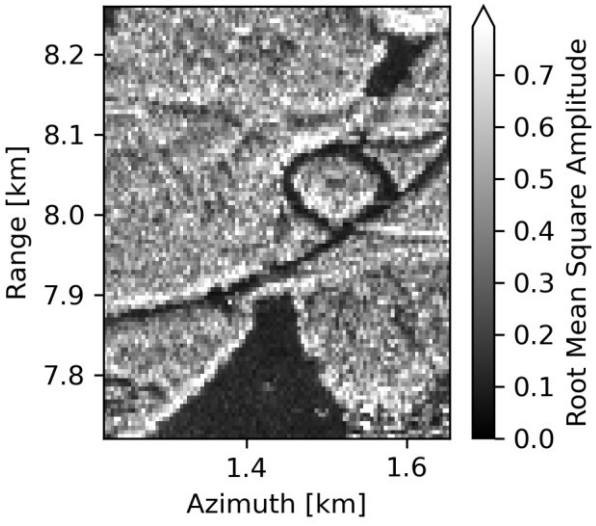

Figure 6 Region of the image formed from track 1 outlined by the red rectangle in **Figure 3** filtered to the [-PRF/2, PRF/2] band. The reported root mean square amplitude was obtained with 9 × 3 pixels in range and azimuth, respectively.

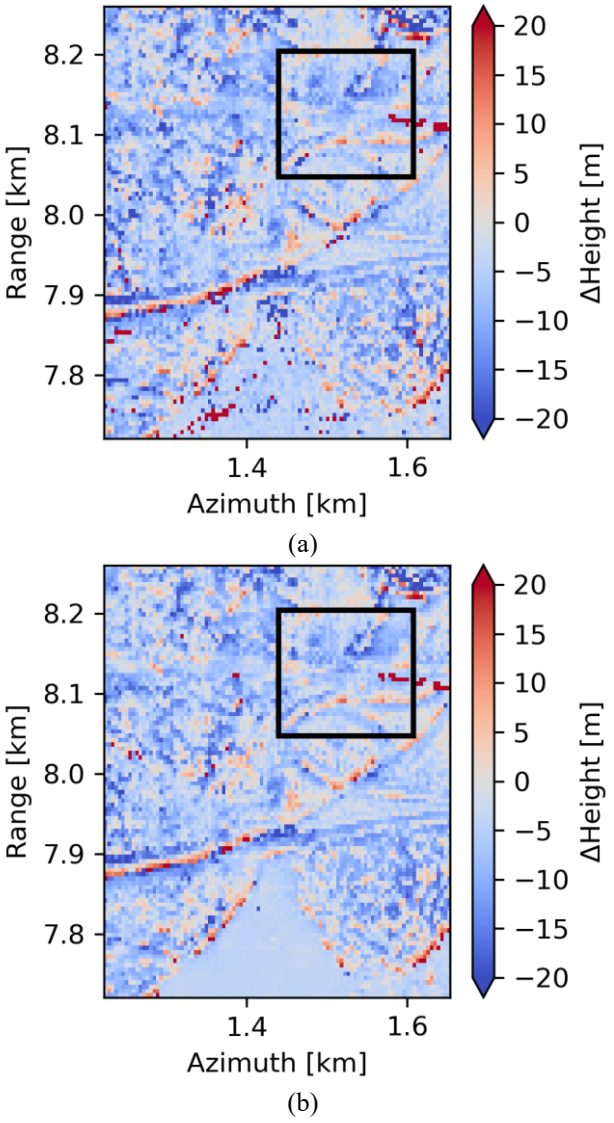

Figure 7 (a) DEM obtained using the generalized maximum likelihood height estimation with the simulated distributed interferometric system. (b) DEM obtained using multi-baseline interferometry with fully-sampled data from tracks 1, 2, 4, 5, and 6, the same tracks used in the simulated distributed interferometric system (see **Figure 5**). The region outlined by the black rectangle was used for the estimation of the statistics of difference between the height measurements of (a) and (b). The indicated height measurements are offsets with respect to the TanDEM-X DEM.

4 Conclusion

This work presents a novel distributed concept that employs a cluster of small-aperture SAR satellites for single-pass generation of highly accurate DEMs robust to unwrapping errors. A key feature of the concept is the generalized maximum likelihood height estimation, which jointly solves the problem of azimuth ambiguities and the non-linear problem of phase ambiguities. This concept generalizes cross-track SAR interferometry to apertures distributed over multiple satellites with a combination of along- and cross-track baselines. The novel processing that supports this concept does not require an intermediate step of image formation and so removes the constraint of arranging the cluster in trains of satellites, enabling further cross-track baseline diversity and allowing fewer satellites to be used.
The first results from a demonstration with airborne data support the theoretical results and shows that the concept is capable of generating DEMs from highly ambiguous SAR images that agree with DEMs generated through conventional multi-baseline SAR interferometry. These first results show negligible bias and a standard deviation of 1.5 m of the difference between the heights estimated with each method in the evaluated region. More comprehensive analyses of the proposed processing technique using larger areas of the dataset will be carried out.
The proposed concept can moreover be seen as a specific formation in a flexible mission that can rearrange the cluster of small-aperture satellites for different applications, such as tomography or along-track interferometry. This concept is an attractive and cost-effective solution for future Earth observation missions for single-pass generation of high-quality DEMs.

5 Funding

Co-funded by the European Union (ERC, DRITUCS, 101076275). Views and opinions expressed are however those of the authors only and do not necessarily reflect those of the European Union or the European Research Council Executive Agency. Neither the European Union nor the granting authority can be held responsible for them.
This work was partially funded by the Deutsche Forschungsgemeinschaft (DFG, German Research Foundation) GRK 2680 – Project-ID 437847244.

6 Literature

[1] R. Bamler and P. Hartl, “Synthetic Aperture Radar Interferometry,” *Inv. Probl.*, vol. 14, no. 4, pp. R1–R54, 1998.

[2] A. Moreira et al., "Tandem-L: A Highly Innovative Bistatic SAR Mission for Global Observation of Dynamic Processes on the Earth's Surface," in *IEEE Geosci. and Rem. Sens. Mag.*, vol. 3, no. 2, pp. 8–23, June 2015.

[3] E. Peral et al., “Radar Technologies for Earth Remote Sensing from CubeSat Platforms,” in *Proceedings of the IEEE*, vol. 106, no. 3, pp. 404–418, March 2018.

[4] G. Krieger et al., “TanDEM-X: A Satellite Formation for High-Resolution SAR Interferometry,” in *IEEE Trans. on Geosci. and Rem. Sens.*, vol. 45, no. 11, pp. 3317–3341, Nov. 2007.

[5] M. Lachaise, T. Fritz and R. Bamler, “The Dual-Baseline Phase Unwrapping Correction Framework for the TanDEM-X Mission Part 1: Theoretical Description and Algorithms,” in *IEEE Trans. on Geosci. and Rem. Sens.*, vol. 56, no. 2, pp. 780–798, Feb. 2018.

[6] M. N. Peixoto, M. Villano, G. Krieger, A. Moreira, C. Waldschmidt, “A Novel Technique to Generate Digital Elevation Models in a Single Pass Using a Cluster of Smallsats,” in *Proc. IGARSS*, Pasadena, CA, USA, Jul. 2023.

[7] M. N. Peixoto, M. Villano, G. Krieger, A. Moreira, “Method for generating digital elevation models of a to-be considered region on earth by using a system of multiple synthetic aperture radar (SAR) platforms,” German Patent Appl. 10 2023 118 442.3, Jul. 12, 2023.

[8] J. Mittermayer, G. Krieger and M. Villano, “Multistatic Dispersed Swarm Configurations for Synthetic Aperture Radar Imaging,” in *IEEE Geosci. and Rem. Sens. Lett.*, vol. 19, pp. 1–5, 2022.

[9] G. Di Martino et al., “Formation-Flying SAR Receivers in Far From Transmitter Geometry: Signal Model and Processing Scheme,” in *Proc. IGARSS*, Brussels, Belgium, 2021, pp. 2711–2714.

[10] A. Renga, A. Gigantino, M. D. Graziano, A. Moccia, A. Fedele and S. Natalucci, “Beamforming and Multi-Platform Image Synthesis for RODiO Distributed SAR Mission,” *73rd International Astronautical Congress (IAC)*, Paris, France, Sep. 2022.

[11] M. Grassi et al, “FORCE: A Formation Flying SAR Based on CubeSat Assemblies,” *73rd International Astronautical Congress (IAC)*, Paris, France, Sep. 2022.

[12] D. Giudici, P. Guccione, D. Mapelli, J. Marini, A. M. Guarnieri, “RAINBOW-SAR: Enhanced Observation Capability by Multiple Frequency Radar,” in *Proc. 7th Workshop on RF and Microwave Systems, Instruments & Sub systems + 5th Ka band Workshop*, May 2022.

[13] N. Sakar, M. Rodriguez-Cassola, P. Prats-Iraola and A. Moreira, “Azimuth Reconstruction Algorithm for Multistatic SAR Formations with Large Along-Track Baselines,” in *IEEE Trans. on Geosci. and Rem. Sens.*, vol. 58, no. 3, pp. 1931–1940, Mar. 2020.

[14] N. Sakar, M. Rodriguez-Cassola, P. Prats-Iraola and A. Moreira, “Sampling Analysis and Processing Approach for Distributed SAR Constellations with Along-Track Baselines,” in *IEEE Trans. on Geosci. and Rem. Sens.*, vol. 60, pp. 1–12, 2022.

[15] M. N. Peixoto, G. Krieger, A. Moreira, C. Waldschmidt and M. Villano, "On the Exploitation of CubeSats for Highly Accurate and Robust Single-Pass SAR Interferometry," in *IEEE Trans. on Geosci. and Rem. Sens.*, 2023.

[16] M. N. Peixoto, M. Villano, G. Krieger, A. Moreira, “Verfahren zur Erkennung und Auflösung von Phasenmehrdeutigkeiten in interferometrischen SAR-Daten,” German Patent Appl. 10 2022 117 088.8, Jul. 8, 2022.

[17] M. Villano and G. Krieger, “Spectral-Based Estimation of the Local Azimuth Ambiguity-to-Signal Ratio in SAR Images,” in *IEEE Trans. on Geosci. and Rem. Sens*., vol. 52, no. 5, pp. 2304–2313, May 2014.

[18] F. Lombardini and P. Lombardo, “Maximum Likelihood Array SAR Interferometry,” *1996 IEEE Digital Signal Processing Workshop Proceedings*, Loen, Norway, 1996, pp. 358–361.